The Madden–Julian Oscillation and Its Impact on Northern Hemisphere Weather Predictability

CHARLES JONES

Institute for Computational Earth System Science, University of California, Santa Barbara, Santa Barbara, California

DUANE E. WALISER

Institute for Terrestrial and Planetary Atmospheres, State University of New York at Stony Brook, Stony Brook, New York

K. M. LAU

Climate and Radiation Branch, NASA Goddard Space Flight Center, Greenbelt, Maryland

W. STERN

Geophysical Fluid Dynamics Laboratory, Princeton University, Princeton, New Jersey

(Manuscript received 21 May 2003, in final form 26 September 2003)

ABSTRACT

The Madden–Julian oscillation (MJO) is known as the dominant mode of tropical intraseasonal variability and has an important role in the coupled-atmosphere system. This study uses numerical model experiments to investigate the influence of the MJO activity on weather predictability in the midlatitudes of the Northern Hemisphere. The National Aeronautics and Space Administration (NASA) Goddard Laboratory for the Atmospheres (GLA) general circulation model was used in a 10-yr simulation with fixed climatological SSTs to generate a control dataset as well as to select initial conditions for active MJO periods and ''Null'' cases. Two perturbation numerical experiments were performed for the 75 cases selected [(4 MJO phases + Null phase) × 15 initial conditions in each]. For each alternative initial condition, the model was integrated for 90 days. Mean anomaly correlations and standardized root-mean-square errors in the midlatitudes of the Northern Hemisphere (20°–60°N) were computed to assess predictability characteristics. The analyses of 500-hPa geopotential height, 200-hPa streamfunction, and 850-hPa zonal wind component systematically show larger predictability (~2–3 days) during periods of active MJO as opposed to quiescent episodes of the oscillation. While further studies are necessary to investigate possible model sensitivity, the results shown here highlight the importance of the MJO in modulating weather variability and show the importance of improving the representation of the MJO in operational numerical weather forecast models.

1. Introduction

The Madden–Julian oscillation (MJO) is known as the dominant mode of tropical intraseasonal variability with characteristic time scales of 30–60 days (Madden and Julian 1994). The MJO, which involves significant variations in tropical convective activity and tropospheric large-scale circulation, is characterized by eastward propagation (e.g., Hendon and Salby 1994; Maloney and Hartmann 1998; Jones et al. 2004). Since the discovery of the oscillation, many studies have demonstrated that tropical–extratropical interactions associated with the MJO can be important as well (Liebmann and Hartmann 1984; Weickmann et al. 1985; Lau and Phillips 1986; Krishnamurti et al. 1997). For example, the MJO strongly influences the precipitation patterns associated with the monsoons in Asia and Australia, and moderately influences those in North America and South America (Yasunari 1979; Lau and Chan 1986; Kiladis and Weickmann 1992; Mo 2000; Nogués-Paegle et al. 2000; Higgins et al. 2000; Higgins and Shi 2001; Jones and Carvalho 2002). Additionally, this influence has been shown to modulate rainfall variability and extreme events in the Americas as well (Higgins et al. 2000; Jones 2000; Bond and Vecchi 2003; Carvalho et al. 2004).

In regards to the strength of the MJO and/or the accuracy of its representation in numerical weather forecast models, a few studies have investigated the poten-

Corresponding author address: Dr. Charles Jones, Institute for Computational Earth System Science, University of California, Santa Barbara, CA 93106.
E-mail: cjones@icess.ucsb.edu

tial role of the MJO in modulating forecast skill in the extratropics. Lau and Chang (1992) analyzed one season of 30-day global forecasts derived from the National Centers for Environmental Prediction (NCEP) forecast model during the Dynamical Extended Range Forecasts (DERF) experiment. Their results showed that the NCEP forecast model has skill in predicting the global pattern of intraseasonal variability up to 10 days, with the error growth of tropical and extratropical low-frequency modes less (greater) than persistence when the amplitude of the MJO is large (small). Using a more recent version of DERF experiments, Hendon et al. (2000) found that forecasts in the Tropics and midlatitudes of the Northern Hemisphere during boreal winter have less skill when they are initialized during or prior to periods of active MJO as opposed to quiescent episodes of the oscillation. They attributed the reduced forecast skill to the inability of the numerical model to sustain the MJO beyond about 7 days, which contributes to erroneous tropical Rossby wave sources. Likewise, skills of medium-range weather forecasts in the Pan-American sector have also been linked to tropical intraseasonal variability (Nogués-Paegle et al. 1998). Jones and Schemm (2000) used NCEP-DERF90 experiments to investigate the influence of the MJO variability in numerical weather forecasts over South America. The results indicated more skill during periods of strong convective activity associated with the MJO as opposed to periods of suppressed or weak activity. The study by Ferranti et al. (1990) followed a different approach and performed a limited set of numerical runs with the European Centre for Medium-Range Weather Forecasts (ECMWF) model to investigate the impacts on extratropical forecasts errors associated with errors in the Tropics. Some of the numerical runs relaxed the tropical atmosphere toward the verifying analysis (perfect tropical prognosis), whereas other experiments were relaxed toward the initial conditions (persistent Tropics). Although their study was based on only four cases of active MJO periods, it clearly suggested the potential impact of the MJO on predictive skill (i.e., comparison of forecasts and observations) in the extratropics.

A key aspect in the issue of investigating the MJO impacts on extratropical weather variability is that previous studies have used global numerical models with notably poor/weak representations of the MJO (Ferranti et al. 1990; Lau and Chang 1992; Hendon et al. 2000; Jones et al. 2000). Furthermore, previous studies that have addressed the impact of MJO variability have done so by assessing forecast skill (Lau and Chang 1992; Hendon et al. 2000; Jones et al. 2000) rather than by examining its effects on midlatitude predictability. The two issues above, together with large errors present in tropical initial conditions, imply that definite conclusions about the influence of the MJO on midlatitude weather predictability are difficult to achieve. Motivated by these considerations, this study uses predictability experiments to investigate the following question: What is the overall influence of MJO activity on weather predictability in the Northern Hemisphere midlatitudes during boreal winter?

2. Model

In order to investigate the influence of the MJO on midlatitude weather predictability, this study uses the exact same model described in Waliser et al. (2003a,b). The numerical model is the National Aeronautics and Space Administration (NASA) Goddard Laboratory for the Atmospheres (GLA) general circulation model (GCM), an earlier version of which is described in Kalnay et al. (1983). Modifications have included increased vertical resolution and several changes in the parameterizations of radiation, convection, cloud formation, precipitation, vertical diffusion, and surface processes (Sud and Walker 1992; Phillips 1996). The horizontal representation uses surface finite differences on a $4^\circ \times 5^\circ$ (latitude $\times$ longitude) energy and momentum conserving A grid (Arakawa and Lamb 1977). The vertical domain has 17 unequally spaced sigma levels extending from the surface to about 12 hPa. Both seasonal and diurnal cycles in the solar forcing are simulated with the atmospheric radiation treatment of Harshvardhan et al. (1987). The formulation of convection follows the scheme of Arakawa and Schubert (1974), as implemented in discrete form by Lord and Arakawa (1980). The model orography is based on the $1^\circ \times 1^\circ$ topographic height data of Gates and Nelson (1975), which has been area averaged over the 40×50 grid boxes. The resulting orography is smoothed using a 16th-order Shapiro (1970) filter and a Fourier filter poleward to 60° latitude.

In general, the GLA model performed very well with respect to its representation of the MJO in the Slingo et al. (1996) Atmospheric Model Intercomparison Project (AMIP) study. Further comparison by Sperber et al. (1996) revealed that the GLA, along with the U.K. Met Office (UKMO) model and version 2 of the Community Climate Model (CCM2), exhibited variability closely resembling the observed features of the MJO. In particular, the GLA model tended to produce a better representation of the eastward propagation of convection and its associated cyclonic and anticyclonic circulation anomalies when compared to the UKMO model. As a first assessment of the MJO influence on midlatitude weather predictability, this study utilizes the fixed-SST version of the model, although simulations with interactive SST by means of a slab ocean showed some modest improvements in the GLA simulation of the MJO (Waliser et al. 1999).

3. Experimental framework

The experimental approach used to examine the MJO influence on weather predictability during extended boreal winter (November–April) was based on a set of

twin predictability experiments (Waliser et al. 2003a). Initial conditions were selected for a number of MJO events from a 10-yr simulation using climatological SSTs. Daily averages (four 6-h values) of a number of fields were saved. The selected MJO events were chosen based on an extended empirical orthogonal function (EEOF) analysis of rainfall data from the region 32°N–32°S, 32.5°E–92.5°W. This region tends to encompass most of the variability in rainfall that is associated with the MJO (e.g., Lau and Chan 1986; Wang and Rui 1990). To isolate the intraseasonal time scale, and thus the MJO, the daily data were first bandpassed with a 30–90-day Lanczos filter (Duchon 1979). EEOF analysis, using temporal lags from -7 to $+7$ pentads, was then performed on pentad averages of the bandpassed rainfall data. The first (second) mode contains 6.0% (5.9%) of the variance of the time-lagged sequences of the bandpassed data. The rainfall variance in the 30–90-day band represents roughly 33% (28%) of the seasonal variance in the Tropics (extratropics).

Candidate MJO events to use for initial conditions were chosen from the amplitude time series associated with model EEOF modes 1 and 2 after having been interpolated to daily values. Given that these modes capture the propagating nature of the MJO, selecting periods when the amplitude of these time series is large will tend to capture strong, propagating MJO events. The two series have maximum correlation (0.95) at a lag of $\pm\sim$12 days indicating a dominant period of about 50 days. When the mode 1 time series is positive (negative), rainfall tends to be high in the western Indian (western Pacific) Ocean, and when the mode 2 time series is positive (negative), rainfall tends to be high in the eastern Indian (central Pacific Ocean/South Pacific convergence zone) Ocean (see Waliser et al. 2003a). Thus, by selecting periods of both positive and negative values of these two series, four separate ''phases'' of the MJO can be distinguished based on the longitudinal position of the heating.

For each of these four phases, the 15 events with the greatest amplitudes for each of the four phases were selected. In order to compare the differences in atmospheric predictability in midlatitude weather between periods of high MJO activity to those with little or no MJO activity, 15 initial conditions were also chosen from periods in which neither of the above modes was strongly exhibited in the model atmosphere. The selection was performed as follows: The amplitude time series for EEOF modes 1–4 for the Northern Hemisphere winter, along with the analogous four series for the summer, were squared, added together, and then smoothed with a 51-day (~MJO cycle) running filter. This combined series gives a bulk index of generalized intraseasonal activity. The 15 events during boreal winter with the lowest values of this index were selected to represent low MJO activity conditions with the additional criteria that the events had to occur at least 10 days apart. The latter criterion was applied in order to get a sample of distinct atmospheric states of low MJO activity [see Waliser et al. (2003a) for details]. Hereafter, these cases will be referred to as ''Null'' events. Figure 1 shows the composites of rainfall for the 15 initial conditions selected for each of the four MJO phases (indicated as Indian, Maritime, W. Pacific, and C. Pacific) as well as the Null events.

Two perturbations were performed for the 75 cases selected [(4 MJO phases + Null phase) $\times$ 15 events]. The perturbation initial conditions were determined as follows: Given the day of the month that the initial condition occurs, day-to-day root-mean-square (rms) differences were computed (on the model's sigma surfaces) from the daily averaged values of the model's four prognostic variables (u, v, T, and q) for that particular month. This process was meant to provide some spatial structure to the perturbation, whereby larger day-to-day variability would translate into more uncertainty in the initial conditions. These rms values were then multiplied by a random number scaled between -0.1 and 0.1 for the first set of perturbations and -0.2 and 0.2 for the second set. These ''errors'' were then added to the original initial condition's prognostic values to produce an alternative initial condition. For each alternative initial condition, the model was integrated for 90 days.

4. Results

The influence of the MJO on boreal winter weather predictability was examined in the following model's variables: 500-hPa geopotential height (Z500), 200-hPa streamfunction (SF200), 850-hPa zonal wind component (U850), and rainfall. Daily anomalies of each of these variables were calculated by subtracting the seasonal cycle determined from the 10-yr fixed SST climatological run. No other filtering was applied to the time series. In the remainder of this section, we contrast the predictability obtained during periods of high MJO activity (120 events: 4 phases $\times$ 15 cases $\times$ 2 perturbations) with low intraseasonal activity or Null cases (30 events: 15 cases $\times$ 2 perturbations).

A number of ways have been proposed to assess forecast skill (Miller and Roads 1990; Déqué and Royer 1992; Wilks 1995). In this study, mean anomaly correlation (acc) (or pattern correlation) was computed as

$$\text{mean acc} = \frac{\langle\overline{(O')(F')}\rangle}{[\langle\overline{(O')^2}\rangle\langle\overline{(F')^2}\rangle]^{1/2}}, \qquad (1)$$

where O' is the ''observed'' daily anomaly from the 10-yr climatological run, and F' is the daily anomaly forecast. Each grid point was weighted by the square root of the cosine of the latitude. Brackets indicate integration over the spatial domain. Although there are different ways of computing mean acc (Déqué and Royer 1992), the arithmetic mean over the sample size is used in this work, which is denoted by overbars. The sample size can be 120 for all MJO cases, 30 for each MJO

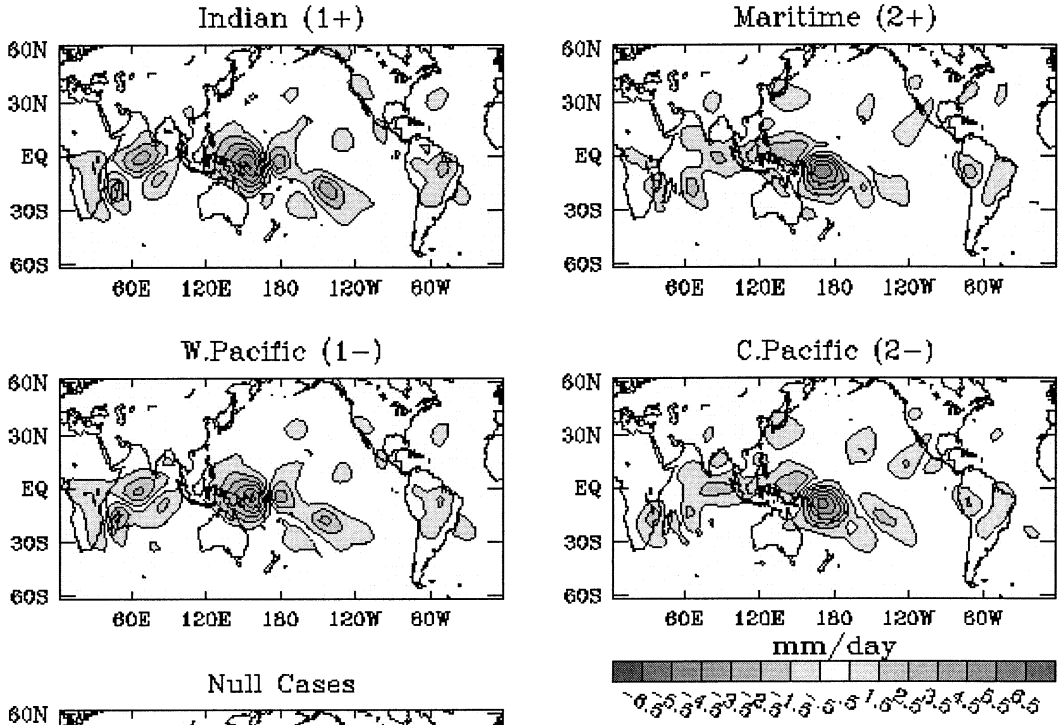

FIG. 1. Composite of filtered (30–90 day) rainfall anomalies for the 15 initial conditions selected to represent the four ''phases'' of the MJO (upper-four panels) as well as the Null cases (lower panel). For example, the upper-left panel [i.e., Indian (1+)] is the average rainfall anomaly from the 15 initial conditions derived from the largest positive amplitudes of the first time series of EEOF analysis (similarly, for the other panels). Except in the Null case (lower left), the headings indicate the geographic region of the most intense MJO-related rainfall as well as the rainfall EEOF mode and sign (e.g., 1+ indicates EEOF mode $1 > 0$).

phase, and 30 for Null cases. In addition, the expression above was calculated for lead times from 1 to 30 days.

Figure 2 shows the mean acc of Z500, SF200, and U850 computed over the Northern Hemisphere midlatitudes (20°–60°N). A common feature shown in the computation of mean acc is the systematically lower predictability obtained during periods of quiescent MJO. For instance, the mean acc of Z500 reaches a value of 0.6 at 15-days lead time during Null cases, whereas the mean acc extends to about 16–18-days lead times during active MJO. In particular, the MJO phase denoted by INDIAN, which corresponds to increased precipitation in the western Indian and central Pacific Oceans (Fig. 1), shows the largest mean acc for all three variables. Note that this study is based on predictability experiments. Operational forecast models usually exhibit acc values of 0.6 by about 7–9-days lead time (Simmons and Hollingsworth 2002).

In order to inspect case-to-case variations and assess the robustness of the predictability experiments, Fig. 3 displays the acc of Z500 (20°–60°N) for each case and perturbation initial conditions contained in the INDIAN MJO phase (left) and Null sample (right) at 5-, 10-, 15-, and 20-days lead time. The horizontal lines indicate the mean acc over all cases at the given lead time (note that the acc scale varies for each lead time). The important point to observe is that, in general, the acc is uniformly distributed across the cases for both INDIAN MJO and Null situations and therefore is not influenced by only a few cases.

An estimate of the statistical significance of differences in mean acc between active MJO and Null cases was achieved with the following procedure. The Fisher transformation (Γ) was first applied to the mean acc at each lead time to ensure a more Gaussian distribution than the mean acc given by (1) (Miller and Roads 1990; Wilks 1995):

$$\Gamma(\tau) = 0.5 \ln\frac{(1 + \rho)}{(1 - \rho)}, \tag{2}$$

where ρ is the mean acc at the lead time τ. Next, the test statistic Z was computed for the differences between Γ in active MJO phases and Null cases at each lead time:

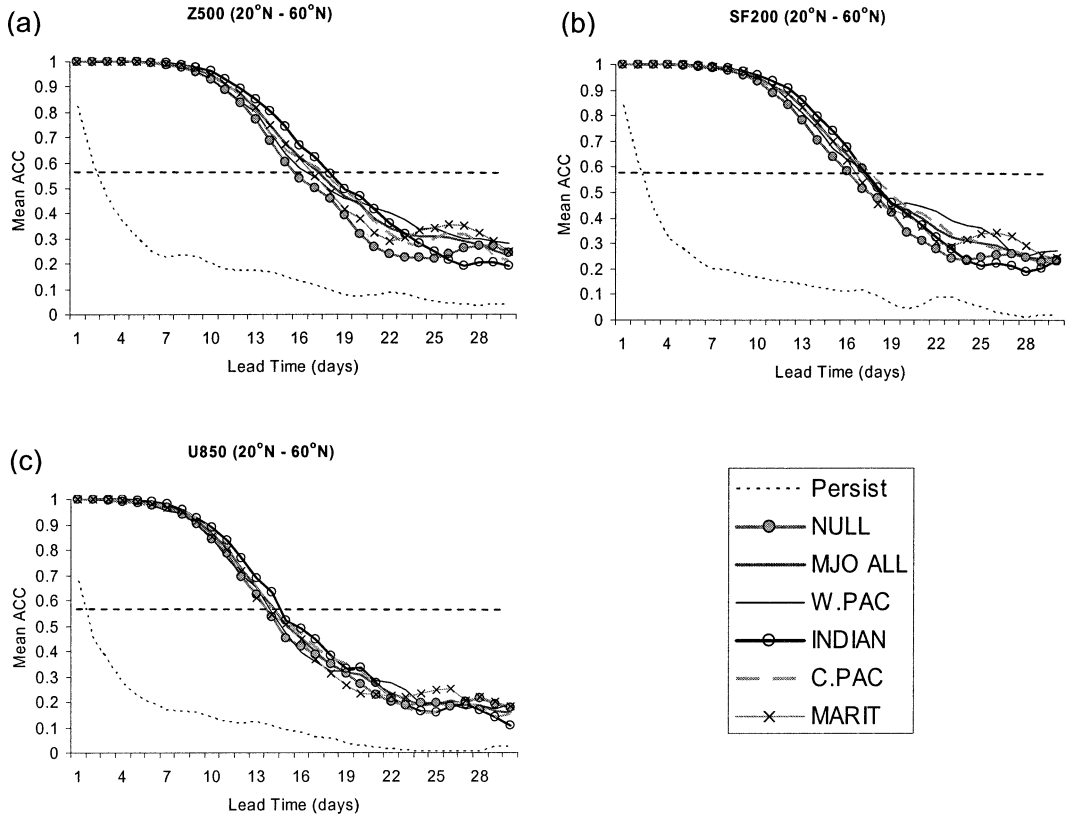

FIG. 2. Boreal winter mean anomaly correlation in the Northern Hemisphere (20°–60°N): (a) geopotential height (500 hPa), (b) streamfunction (200 hPa), and (c) zonal component of the wind (850 hPa). Anomaly correlations are averaged over all model run cases in each phase of the MJO and Null cases (see text for details).

$$Z = \frac{(\Gamma_{\mathrm{MJO}} - \Gamma_{\mathrm{null}})}{\sqrt{\dfrac{\sigma^2_{\mathrm{MJO}}}{N_{\mathrm{MJO}}} + \dfrac{\sigma^2_{\mathrm{null}}}{N_{\mathrm{null}}}}}, \tag{3}$$

where σ is the variance of Γ, and N is the number of cases. Figure 4 shows the Z statistic at lead times from 10 to 15 days for Z500, SF200, and U850 and each MJO phase. Values of Z greater than 1.96 (1.64) indicate that differences in Γ are statistically significant at 95% (90%) level. Thus, the results based on mean acc suggest higher weather predictability in the Northern Hemisphere midlatitudes during the active INDIAN phase of MJO relative to quiescent episodes of the oscillation.

Another way of estimating predictability is the rms error between control and perturbation simulations. Since the variance during periods of active MJO and Null situations can be significantly different in the midlatitudes of the Northern Hemisphere, a standardized rms error was computed by normalizing each time series of control and perturbation by the mean and standard deviation of the control case. For instance, for any selected initial condition, the control run time series (O') was normalized as $O_S = (O' - \overline{O})/\sigma$, where $\overline{O}$ and σ are the mean and standard deviation of O' computed over a 120-day window around the initial condition (30 days before and 90 days after the initial condition). Similarly, the perturbation (F') run was normalized as $F_S = (F' - \overline{O})/\sigma$.

Figure 5 shows the standardized rms error, spatially averaged from 20° to 60°N, for the fields of Z500, SF200, and U850. Higher predictability is obtained during active MJO situations than in the Null cases. In agreement with results shown before, the INDIAN phase associated with active MJO cases exhibits the highest skill. For example, while the standardized rms error in Z500 reaches a value of 1 at 15-days lead time in the Null cases, the rms error attains a value of 1 at about 18-days lead time during the INDIAN phase.

The influence of the MJO on boreal winter weather predictability was further investigated by examining the mean acc between control and perturbation runs of rainfall during active MJO and Null cases. Three domains (Fig. 6, bottom right) were chosen: tropical Indian Ocean and western Pacific, western North America, and eastern South America. These regions were selected given that observational studies have related the eastward propagation of the MJO with significant changes in rainfall in those areas (Yasunari 1979; Lau and Chan 1986; Mo 2000; Nogués-Paegle et al. 2000; Higgins and Shi 2001; Jones and Carvalho 2002; Higgins et al. 2000;

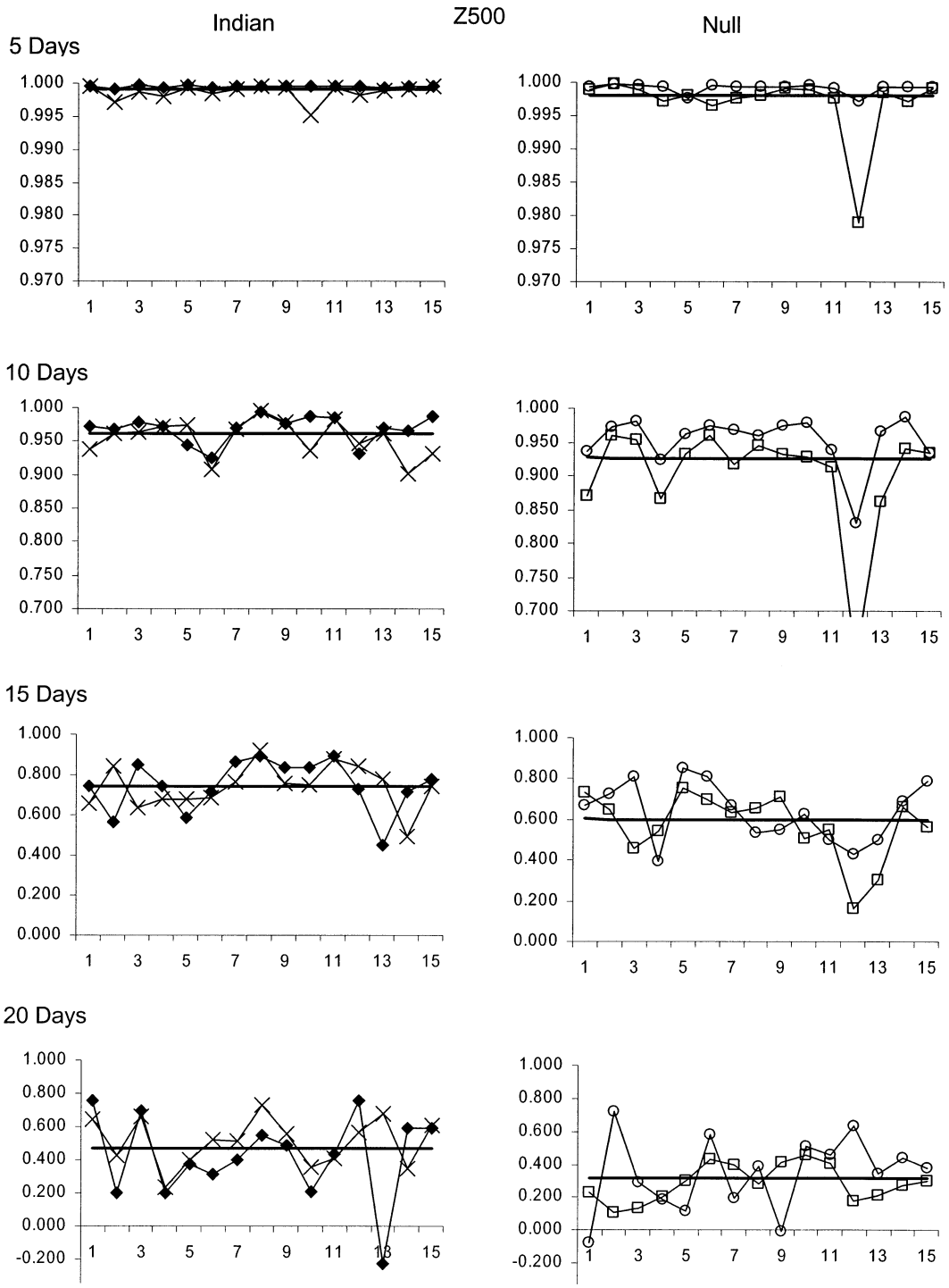

FIG. 3. Boreal winter anomaly correlation of Z500 in the Northern Hemisphere (20°–60°N). Anomaly correlations are shown for each model run experiment for (left) active MJO in the Indian Ocean and (right) Null cases. Lead times are displayed from 5 to 20 days. Thick horizontal lines indicate the average of the anomaly correlation at the given lead time.

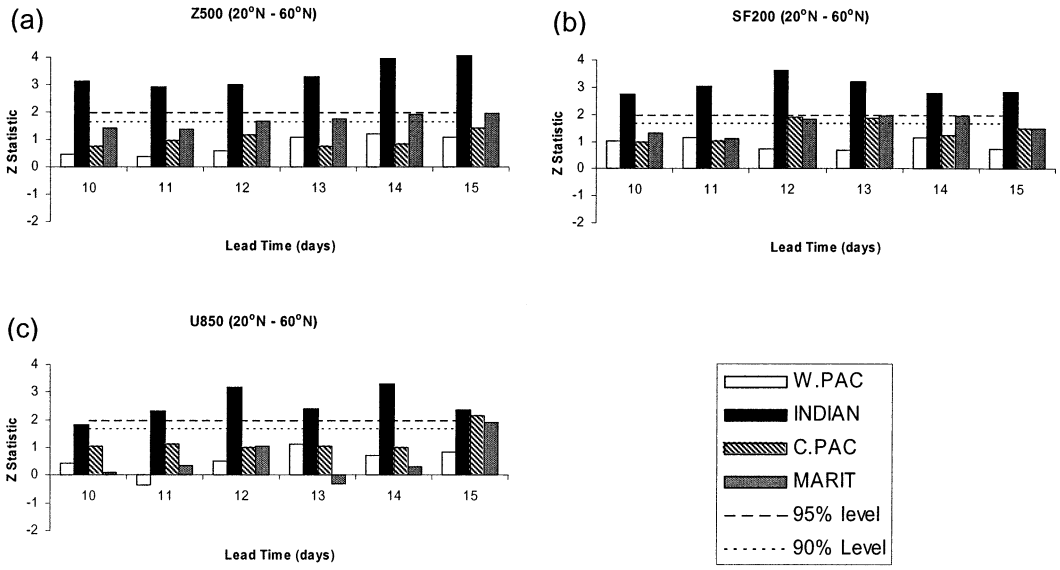

FIG. 4. The *Z* test statistic of difference in boreal winter mean anomaly correlation between active MJO and Null situations. Short- and long-dash horizontal lines indicate 90% and 95% significance levels, respectively.

Jones 2000; Carvalho et al. 2004). Figure 6 displays the mean acc of rainfall over the selected regions. It is interesting to note that there are no major differences in mean acc during active MJO and quiescent periods in these regions, which perhaps results from the more stochastic nature of rainfall variability as compared to large-scale dynamics.

5. Summary and conclusions

It has been recognized for some time that tropical atmospheric processes, primarily involving latent heating due to organized convective activity, can force the tropical large-scale circulation and excite modes that can propagate into the extratropics. A large number of observational studies, for instance, have identified teleconnection processes on intraseasonal (e.g., Liebmann and Hartmann 1984; Weickmann et al. 1985; Lau and Phillips 1986; Krishnamurti et al. 1997) and interannual time scales (e.g., Horel and Wallace 1981; Wallace and Gutzler 1981). The theoretical basis has been described in several studies (e.g., Hoskins and Karoly 1981; Simmons et al. 1983).

In contrast, the predictability of the atmosphere in the midlatitudes depends on internal dynamics of the midlatitudes' variability and modulation by tropical forcing (Qin and Robinson 1995). Simply because a given large-scale tropical convective heating can generate a signal in the extratropics does not necessarily mean a significant impact on forecast skill (and predictability) in the midlatitudes (Qin and Robinson 1995; Kumar and Hoerling 1995). In regards to the MJO, Bladé and Hartmann (1995), for instance, indicate that the spatial structure of the tropical forcing, its time scale, and its eastward propagation are quite important in generating a midlatitude response that stands out above the background variability.

This study used numerical model experiments to investigate the influence of the MJO activity on weather predictability in the midlatitudes of the Northern Hemisphere during boreal winter. The NASA GLA general circulation model was first used in a 10-yr simulation with fixed climatological SSTs to generate a control run as well as to select initial conditions for active MJO periods and Null cases. Two perturbation numerical experiments were performed for the 75 cases selected [(4 MJO phases + Null phase) $\times$ 15 initial conditions in each]. For each alternative initial condition, the model was integrated for 90 days. Mean anomaly correlations in the midlatitudes of the Northern Hemisphere (20°–60°N) and standardized rms errors were computed to assess predictability. The analyses of Z500, SF200, and U850 fields systematically show larger predictability of about 2–3 days during periods of active MJO as opposed to quiescent episodes of the oscillation. These results are in agreement with the increased predictive skill obtained during situations of amplified tropical intraseasonal variability discussed by Ferranti et al. (1990) and Lau and Chang (1992).

It is also important to recognize a number of caveats. First, while the intraseasonal peak of equatorial wavenumber 1, upper-level velocity potential, and zonal wind in the model is quite similar in terms of magnitude and frequency to observations, the model spectra has too much high-frequency (~days) variability for wavenumber 1 (Slingo et al. 1996). Relative to the MJO, this variability would be considered unorganized, that is, errant convective activity that may erode the relatively smooth evolution of the MJO. Second, these simulations were carried out with fixed climatological SST values.

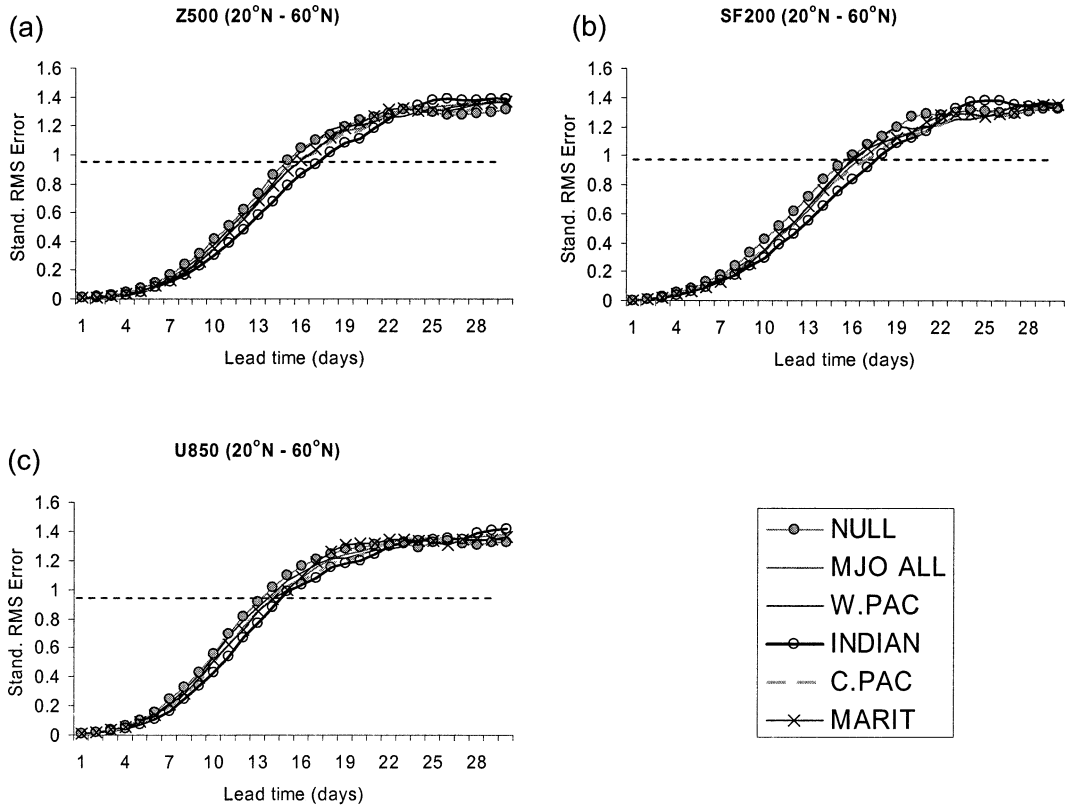

FIG. 5. Boreal winter mean standardized rms error in the Northern Hemisphere (20°–60°N): (a) geopotential height (500 hPa), (b) streamfunction (200 hPa), and (c) zonal component of the wind (850 hPa).

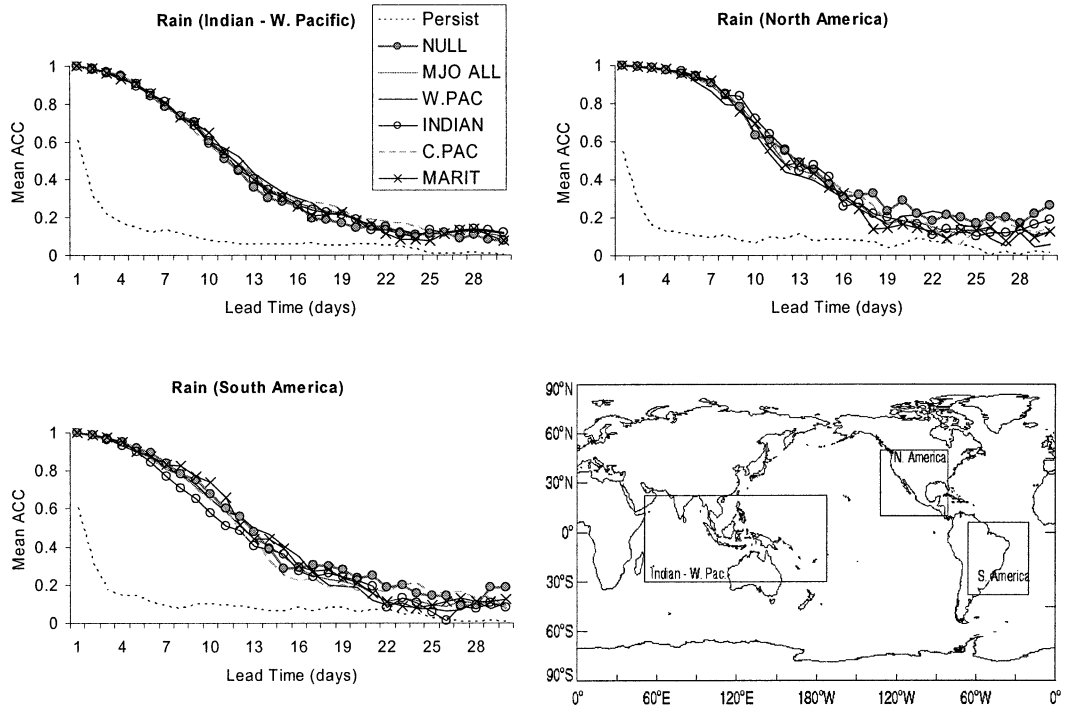

FIG. 6. Boreal winter mean anomaly correlation of rainfall. Anomaly correlations are computed in the three regions indicated on the bottom right and are averaged over all model run cases in each phase of the MJO and Null cases.

A previous study with this model showed that coupled SSTs tend to have an enhancing and organizing influence on the MJO, making it stronger and more coherent (Waliser et al. 1999). The third aspect is the fact that the model contains too little variability over the western Indian Ocean and southern Maritime Continent region. It is interesting to observe, however, that the MJO phase corresponding to enhanced precipitation in the Indian and western Pacific Oceans (INDIAN) is associated with the largest predictability sensitivity found with this numerical model. Further experiments are necessary to better identify the exact location of enhanced tropical precipitation associated with active MJO that have the largest impact on weather predictability. In this regard, the importance of the MJO modulating weather predictability during boreal summer has also been investigated using the NASA GLA model, although in that case no significant modulation was found between strong and weak MJO cases.

Observational studies have extensively indicated a significant role of the MJO on rainfall variability in the Tropics and extratropical regions of the Americas. While the predictability experiments shown here indicate an MJO impact on boreal winter large-scale circulation (Z500, SF200, and U850), the influence of active MJO periods on rainfall predictability is less clear (Fig. 6). In our current research, we are examining this topic further, including a possible modulation of the MJO on the predictability of extreme rainfall events, influence of El Niño–Southern Oscillation, and model sensitivity.

Acknowledgments. The authors would like to acknowledge the support of the following research grants: C. Jones, National Science Foundation (ATM-0094387) and NOAA Office of Global Programs CLIVAR–Pacific Program (NA16GP1019) and CLIVAR-PACS (NA16GP1020); D. E. Waliser, National Science Foundation (ATM-0094416) and NOAA Office of Global Programs CLIVAR (NA16GP2021).

REFERENCES

Arakawa, A., and W. H. Schubert, 1974: Interaction of a cumulus cloud ensemble with the large-scale environment, Part I. *J. Atmos. Sci.,* **31,** 674–701.

——, and V. R. Lamb, 1977: Computational design of the basic dynamical processes of the UCLA general circulation model. *Methods in Computational Physics,* J. Chang, Ed., Vol. 17, Academic Press, 173–265.

Bladé, I., and D. L. Hartmann, 1995: The linear and nonlinear extratropical response of the atmosphere to tropical intraseasonal heating. *J. Atmos. Sci.,* **52,** 4448–4471.

Bond, N. A., and G. A. Vecchi, 2003: The influence of the Madden–Julian oscillation on precipitation in Oregon and Washington. *Wea. Forecasting,* **18,** 600–613.

Carvalho, L. M., C. Jones, and B. Liebmann, 2004: The South Atlantic convergence zone: Intensity, form, persistence, and relationships with intraseasonal to interannual activity and extreme rainfall. *J. Climate,* **17,** 88–108.

Déqué, M., and J. F. Royer, 1992: The skill of extended-range extratropical winter dynamical forecasts. *J. Climate,* **5,** 1346–1356.

Duchon, C. E., 1979: Lanczos filter in one and two dimensions. *J. Appl. Meteor.,* **18,** 1016–1022.

Ferranti, L., T. N. Palmer, F. Molteni, and K. Klinker, 1990: Tropical–extratropical interaction associated with the 30–60 day oscillation and its impact on medium and extended range prediction. *J. Atmos. Sci.,* **47,** 2177–2199.

Gates, W. L., and A. B. Nelson, 1975: A new (revised) tabulation of the Scripps topography on a one-degree global grid. Part 1: Terrain heights. Tech. Rep. R-1276-1-ARPA, The Rand Corporation, Santa Monica, CA, 132 pp.

Harshvardhan, R. Davies, D. A. Randall, and T. G. Corsetti, 1987: A fast radiation parameterization for general circulation models. *J. Geophys. Res.,* **92,** 1009–1026.

Hendon, H. H., and M. L. Salby, 1994: The life cycle of the Madden–Julian oscillation. *J. Atmos. Sci.,* **51,** 2225–2237.

——, B. Liebmann, M. Newman, J. D. Glick, and J. Schemm, 2000: Medium-range forecast errors associated with active episodes of the Madden–Julian oscillation. *Mon. Wea. Rev.,* **128,** 69–86.

Higgins, R. W., and W. Shi, 2001: Intercomparison of the principal modes of interannual and intraseasonal variability of the North American monsoon system. *J. Climate,* **14,** 403–417.

——, J.-K. E. Schemm, W. Shi, and A. Leetmaa, 2000: Extreme precipitation events in the western United States related to tropical forcing. *J. Climate,* **13,** 793–820.

Horel, J. D., and J. M. Wallace, 1981: Planetary-scale atmospheric phenomena associated with the Southern Oscillation. *Mon. Wea. Rev.,* **109,** 813–829.

Hoskins, B. J., and D. Karoly, 1981: The steady linear response of a spherical atmosphere to thermal and orographic forcing. *J. Atmos. Sci.,* **38,** 1179–1196.

Jones, C., 2000: Occurrence of extreme precipitation events in California and relationships with the Madden–Julian oscillation. *J. Climate,* **13,** 3576–3587.

——, and J.-K. E. Schemm, 2000: The influence of intraseasonal variations on medium-range weather forecasts over South America. *Mon. Wea. Rev.,* **128,** 486–494.

——, and L. M. V. Carvalho, 2002: Active and break phases in the South American monsoon system. *J. Climate,* **15,** 905–914.

——, D. E. Waliser, J. K. Schemm, and W. K. Lau, 2000: Prediction skill of the Madden–Julian oscillation in dynamical extended range forecasts. *Climate Dyn.,* **16,** 273–289.

——, L. M. V. Carvalho, W. Higgins, D. Waliser, and J-K. Schemm, 2004: Climatology of tropical intraseasonal convective anomalies: 1979–2002. *J. Climate,* **17,** 523–539.

Kalnay, E., R. Balgovind, W. Chao, D. Edelmann, J. Pfaendtner, L. Takacs, and K. Takano, 1983: Documentation of the GLAS fourth-order general circulation model. NASA Tech. Memo. 86064, Vol. 1, NASA Goddard Space Flight Center, Greenbelt, MD, 436 pp.

Kiladis, G. N., and K. M. Weickmann, 1992: Circulation anomalies associated with tropical convection during northern winter. *Mon. Wea. Rev.,* **120,** 1900–1923.

Krishnamurti, T. N., M. C. Sinha, V. Misra, and O. P. Sharma, 1997: Tropical–middle latitude interactions viewed via wave energy flux in the frequency domain. *Dyn. Atmos. Oceans,* **27,** 383–412.

Kumar, A., and M. P. Hoerling, 1995: Prospects and limitations of seasonal atmospheric GCM predictions. *Bull. Amer. Meteor. Soc.,* **76,** 335–345.

Lau, K. M., and P. H. Chan, 1986: Aspects of the 40–50 day oscillation during the northern summer as inferred from outgoing longwave radiation. *Mon. Wea. Rev.,* **114,** 1354–1367.

——, and T. J. Phillips, 1986: Coherent fluctuations of extratropical geopotential height and tropical convection in intraseasonal time scales. *J. Atmos. Sci.,* **43,** 1164–1181.

——, and F. C. Chang, 1992: Tropical intraseasonal oscillation and its prediction by the NMC operational model. *J. Climate,* **5,** 1365–1378.

Liebmann, B., and D. L. Hartmann, 1984: An observational study of

tropical–midlatitude interaction on intraseasonal time scales during winter. *J. Atmos. Sci.,* **41,** 3333–3350.

Lord, S. J., and A. Arakawa, 1980: Interaction of a cumulus cloud ensemble with the large-scale environment. Part II. *J. Atmos. Sci.,* **37,** 2677–2962.

Madden, R. A., and P. R. Julian, 1994: Observation of the 40–50-day tropical oscillation—A review. *Mon. Wea. Rev.,* **122,** 814–837.

Maloney, E. D., and D. L. Hartmann, 1998: Frictional moisture convergence in a composite life cycle of the Madden–Julian oscillation. *J. Climate,* **11,** 2387–2403.

Miller, A. J., and J. O. Roads, 1990: A simplified coupled model of extended-range predictability. *J. Climate,* **3,** 523–542.

Mo, K. C., 2000: Intraseasonal modulation of summer precipitation over North America. *Mon. Wea. Rev.,* **128,** 1490–1505.

Nogués-Paegle, J., K. Mo, and J. Paegle, 1998: Predictability of the NCEP–NCAR reanalysis model during austral summer. *Mon. Wea. Rev.,* **126,** 3135–3152.

——, L. A. Byerle, and K. Mo, 2000: Intraseasonal modulation of South American summer precipitation. *Mon. Wea. Rev.*, **128,** 837–850.

Phillips, T. J., 1996: Documentation of the AMIP models on the World Wide Web. *Bull. Amer. Meteor. Soc.,* **77,** 1191–1196.

Qin, J., and W. A. Robinson, 1995: The impact of tropical forcing on extratropical predictability in a simple global model. *J. Atmos. Sci.,* **52,** 3895–3910.

Shapiro, R., 1970: Smoothing, filtering and boundary effects. *Rev. Geophys. Space Phys.,* **8,** 359–387.

Simmons, A. J., and A. Hollingsworth, 2002: Some aspects of the improvement in skill of numerical weather prediction. *Quart. J. Roy. Meteor. Soc.,* **128,** 647–677.

——, J. M. Wallace, and G. W. Branstator, 1983: Barotropic wave propagation and instability, and atmospheric teleconnection patterns. *J. Atmos. Sci.,* **40,** 1363–1392.

Slingo, J. M., and Coauthors, 1996: Intraseasonal oscillations in 15 atmospheric general circulation models: Results from an AMIP diagnostic subproject. *Climate Dyn.,* **12,** 325–357.

Sperber, K. R., J. M. Slingo, P. M. Inness, and K.-M. Lau, 1996: On the maintenance and initiation of the intraseasonal oscillation in the NCEP/NCAR reanalysis and the GLA and UKMO AMIP simulations. *Climate Dyn.,* **13,** 769–795.

Sud, Y. C., and G. K. Walker, 1992: A review of recent research on improvement of physical parameterizations in the GLA GCM. *Physical Processes in Atmospheric Models,* D. R. Sikka and S. S. Singh, Eds., Wiley Eastern, 422–479.

Waliser, D. E., K. M. Lau, and J.-H. Kim, 1999: The influence of coupled sea surface temperatures on the Madden–Julian oscillation: A model perturbation experiment. *J. Atmos. Sci.,* **56,** 333–358.

——, K. M. Lau, W. Stern, and C. Jones, 2003a: Potential predictability of the Madden–Julian oscillation. *Bull. Amer. Meteor. Soc.,* **84,** 33–50.

——, W. Stern, S. Schubert, and K. M. Lau, 2003b: Dynamic predictability of intraseasonal variability associated with the Asian summer monsoon. *Quart. J. Roy. Meteor. Soc.,* **129,** 2897–2925.

Wallace, J. M., and D. S. Gutzler, 1981: Teleconnections in the geopotential height field during the Northern Hemisphere winter. *Mon. Wea. Rev.,* **109,** 784–812.

Wang, B., and H. Rui, 1990: Synoptic climatology of the transient tropical intraseasonal convection anomalies. *Meteor. Atmos. Phys.,* **44,** 43–61.

Weickmann, K. M., G. R. Lussky, and J. E. Kutzbach, 1985: Intraseasonal (30–60 day) fluctuations of outgoing longwave radiation and 250 mb streamfunction during northern winter. *Mon. Wea. Rev.,* **113,** 941–961.

Wilks, D. S., 1995: *Statistical Methods in the Atmospheric Sciences.* Academic Press, 464 pp.

Yasunari, T., 1979: Cloudiness fluctuations associated with the Northern Hemisphere summer monsoon. *J. Meteor. Soc. Japan,* **57,** 225–229.